

Article

Yb-ASE Suppression in Single-Frequency Hybrid Double Cladding Erbium–Ytterbium Co-Doped Fiber Amplifier with SMS Structure

Xiaolei Bai *, Meng Wang, Yuxing Yang, Zhiguo Lv and Weiguo Jia

School of Physical Science and Technology, Inner Mongolia University, Hohhot 010021, China; wangmeng@imu.edu.cn (M.W.); yuxingyang@imu.edu.cn (Y.Y.); lvzhiguo@imu.edu.cn (Z.L.); jwg1960@163.com (W.J.)

* Correspondence: baixiaolei@imu.edu.cn

Abstract: A hybrid double cladding erbium–ytterbium co-doped fiber (EYDF) amplifier with a single-mode-multimode-single-mode (SMS) active fiber is demonstrated in this study. The hybrid gain fiber with an SMS structure is composed of two kinds of EYDFs with 6 and 12 μm core diameters. The transmission spectra of the SMS fiber structure were theoretically analyzed and the simulation results indicated that the maximum loss in the 1~1.1 μm band where the Yb-band amplified spontaneous emission (Yb-ASE) located, was much larger than that of the 1.5- μm band because of the wavelength difference. The power performance and spectra properties of the hybrid fiber amplifier were theoretically and experimentally analyzed and compared with a typical uniform fiber amplifier under the same conditions. The experimental results demonstrated that this hybrid fiber amplifier can suppress the Yb-ASE by over 12 dB and increase the slope efficiency by more than 2%, but the ASE in the 1.5- μm band increases by 2~3 dB. This work provides a possible method to enable EYDF amplifiers to suppress the Yb-ASE and overcome the pump bottleneck effect.

Keywords: fiber amplifier; erbium–ytterbium co-doped fiber; amplified spontaneous emission; SMS structure



Citation: Bai, X.; Wang, M.; Yang, Y.; Lv, Z.; Jia, W. Yb-ASE Suppression in Single-Frequency Hybrid Double Cladding Erbium–Ytterbium Co-Doped Fiber Amplifier with SMS Structure. *Appl. Sci.* **2021**, *11*, 9334. <https://doi.org/10.3390/app11199334>

Academic Editors: Zhenxu Bai, Qiang Wu and Quan Sheng

Received: 7 September 2021
Accepted: 7 October 2021
Published: 8 October 2021

Publisher's Note: MDPI stays neutral with regard to jurisdictional claims in published maps and institutional affiliations.



Copyright: © 2021 by the authors. Licensee MDPI, Basel, Switzerland. This article is an open access article distributed under the terms and conditions of the Creative Commons Attribution (CC BY) license (<https://creativecommons.org/licenses/by/4.0/>).

1. Introduction

A single-frequency fiber laser at 1.55 μm wavelength with narrow linewidth, low fiber transmission loss, and eye-safe properties has great application in many fields, such as LIDAR, coherence optical communication, high sensitivity fiber sensors, and so on [1,2]. The erbium–ytterbium co-doped fiber (EYDF) amplifier is the main method for obtaining a high-power single-frequency laser because it can minimize the linewidth broadening. Compared with the erbium-doped fiber amplifier (EDFA), the amplifier with erbium–ytterbium co-doped fiber as a gain medium achieves high amplification efficiency by doping Yb-ions. In 2005, Jeong et al. demonstrated a high-power EYDF amplifier and obtained a 151 W single-frequency fiber laser with megahertz level linewidth [3]. We also obtained a 56.4 W high power 1.55 μm fiber laser with a linewidth of 4.2 kHz through an EYDF amplifier in 2015 [4]. However, the Yb-band amplified spontaneous emission (Yb-ASE) in the EYDF with a wavelength range of 1000~1100 nm, not only affects the output signal-to-noise ratio (SNR) but also limits the amplification efficiency of the Er-band signal light. When the pump rate exceeds the cross-relaxation rate between Yb^{3+} and Er^{3+} ions, or in high power pump conditions, the upper-level population of Yb^{3+} ions will accumulate and the Yb-ASE intensity will increase rapidly. This phenomenon, known as the pump bottleneck effect can reduce the conversion efficiency of the pump energy to Er-band signal and can become an important limitation in the power scaling, besides the stimulated Brillouin scattering (SBS). In 2007, the bottleneck effect was observed for the first time in an erbium–ytterbium co-doped fiber oscillator by Jeong et al. [5] and it has attracted the interest of researchers since then. Several effective Yb-ASE suppression methods have

been reported in recent years. In 2010, Kuhn et al. demonstrated that an auxiliary laser with a wavelength in the Yb-band injected in the EYDF and amplified with Er-band signal, together can avoid the accumulation of Yb-ions upper-level population [6]. In 2011 and 2012, Sobon et al. realized Yb-ASE suppression by reflecting part of backward Yb-ASE [7] or constructing a Yb-band ring resonator [8]. This auxiliary 1- μm laser feedback method used in the EYDF amplifier was theoretically analyzed by Han et al. in 2011 [9]. They also experimentally obtained 40.4% slope efficiency by using FBG feedback partial backward Yb-ASE in 2015 [10]. Although the feedback of auxiliary 1- μm signal can effectively reduce the intensity of Yb-ASE, this method needs additional components or laser source, which will increase the cost and insertion loss of the amplifier. Another effective way to improve the limitation of the bottleneck effect is by optimizing the pump wavelength. In 2016, Creeden et al. obtained the record highest output power (207 W) for a single-frequency 1560 nm fiber laser by using the 940-nm LD as the pump source [11]. The corresponding slope efficiency was 50.5%, which is also the highest efficiency for the EYDF amplifier up to now. The relationship between the pump wavelength and the intensity of Yb-ASE was simulated and analyzed by Booker et al. in 2018, which provided a theoretical basis for optimizing the pump wavelength [12]. However, the commercial LD with specially optimized wavelength output is too expensive to be widely used. A simple structure, low-cost method is needed to suppress Yb-ASE effectively and improve the efficiency of the EYDF amplifier.

In addition, the single-mode-multimode-single-mode (SMS) fiber structure has been widely researched because of its simple structure, low cost, and easy adjustment of output spectra [13,14]. Due to the sensitivity of the environmental parameters, the SMS fiber structure is also used in sensing temperature [15], stress [16], vibration [17], the refractive index [18,19], and so on. The multimode interference (MMI) effects in the multimode fiber segment causes output spectral modulation of the SMS structure. The transverse modes excited in the multimode fiber segment are coherently superimposed at the fusion point of the output end single-mode fiber. Due to this MMI effect, the number of excited transverse modes, which is related to the fiber core diameter, determines the coherence intensity, and then affects the modulation depth of the output spectrum [20]. In step-index fiber, the normalized frequency V is inversely proportional to the wavelength λ and directly proportional to the mode number N [21]. The laser with a shorter wavelength can excite more transverse modes in the same core diameter fiber. It can be inferred that the laser with a shorter wavelength can obtain greater modulation depth in a specific SMS structure. Specifically, in EYDF amplifiers, the Yb-ASE with a wavelength near 1 μm can result in more transmission loss than the Er-ASE with a wavelength range of 1500~1600 nm, when propagating through an SMS structure. This provides a possible way to suppress Yb-ASE in EYDF amplifiers by using an SMS structure. Although the SMS fiber structure made with passive fiber can be used as a bandpass filter [21,22], the increment in fiber length caused by insertion in the structure is disadvantageous to the fiber amplifier as it suppresses the nonlinear effect, especially the SBS. In our previous work, two fibers with different core diameters were spliced together to suppress reverse propagating light [23]. If the SMS structure can be made from commercial gain fiber with different core diameters, it could filter the ASE while providing gain without increasing the total length of the amplifier. However, there are two limitations to the usage of SMS structures based on active fiber. One reason is that the core size of commercial double cladding gain fiber is too small to obtain significant MMI effects at their working wavelength. The other is that the fusion point on the gain fiber will reduce the thermal stability of the amplifier. Broadening the working wavelength range or considering other light with a shorter wavelength could obtain sufficient modes to achieve an obvious MMI effect, while the second problem can be reduced by fiber thermal management.

In this work, we attempted to make an SMS structure by using commercial EYDF with different core diameters, and analyzed its properties in an amplifier, not only at the signal but also the Yb-ASE band. A single-frequency hybrid erbium–ytterbium co-doped fiber amplifier with an SMS structure is proposed. Two kinds of EYDFs with core diameters of 6 and 12 μm were spliced in sequence to form a hybrid gain fiber with an SMS structure. The output performance of the hybrid EYDF amplifier was numerically and experimentally analyzed. The length of multimode fiber in the SMS structure was preliminarily optimized by simulation. The experimental results demonstrated that compared with a typical uniform EYDF amplifier, the hybrid EYDF amplifier with the same fiber length can suppress the Yb-ASE by over 12 dB without any reduction in output power. The efficiency of the amplifier can be improved by 2.7% because of Yb-ASE suppression and the additional gain provided by the SMS active fiber structure. This provides a monolithic structure for the EYDF amplifier to overcome the pump bottleneck effect and achieves high efficiency and high-power output.

2. Experimental Setup

A schematic diagram of the single-frequency hybrid EYDF amplifier is shown in Figure 1. The seed laser is a homemade single-frequency fiber laser with a central wavelength of 1550.14 nm and output power of 30 mW. The linewidth of this seed fiber laser is 630 Hz [24]. The seed laser is coupled into hybrid gain fiber via an isolator and a $(2 + 1) \times 1$ combiner in sequence. The isolation coefficient of the isolator is 40 dB and the max insertion loss is 0.3 dB. The output power after the isolator is 28 mW. The hybrid gain fiber consists of SM-EYDF-6/125 (Nufern, SM-EYDF-6/125-HE) and MM-EYDF-12/130 (Nufern, MM-EYDF-12/130-HE). The cladding absorption of these active fibers is 1.8 and 4 dB/m at 976 nm, respectively. Three EYDF segments are spliced in the order of SM-6/125, MM-12/130, and SM-6/125 to form an SMS structure in the core. However, the difference in the inner cladding diameters of these fibers is tiny, so there is no additional transmission loss for the inner cladding pump light passing without fusion loss. To keep the amplifier stable and avoid the influence of fiber temperature on the output spectrum of the SMS structure [25,26], the whole gain fiber is placed on a water-cooled heat sink for heat dissipation. The 976-nm pump laser and input signal are forward coupled into the gain fiber through the pump combiner, which is shown in the dotted box in Figure 1. The residual pump is stripped out by a homemade cladding light stripper (CLS) at the end of the gain fiber. The output pigtail of the amplifier is angle cleaved to launch the signal. A typical EYDF amplifier with uniform gain fiber was theoretically and experimentally investigated for comparison with a hybrid EYDF amplifier. The basic structure and the gain fiber length of this typical amplifier is the same as those of the hybrid amplifier, except that the gain fiber is uniform SM-EYDF-6/125. For the convenience of the reader, the structural diagram of the typical EYDF amplifier is omitted here.

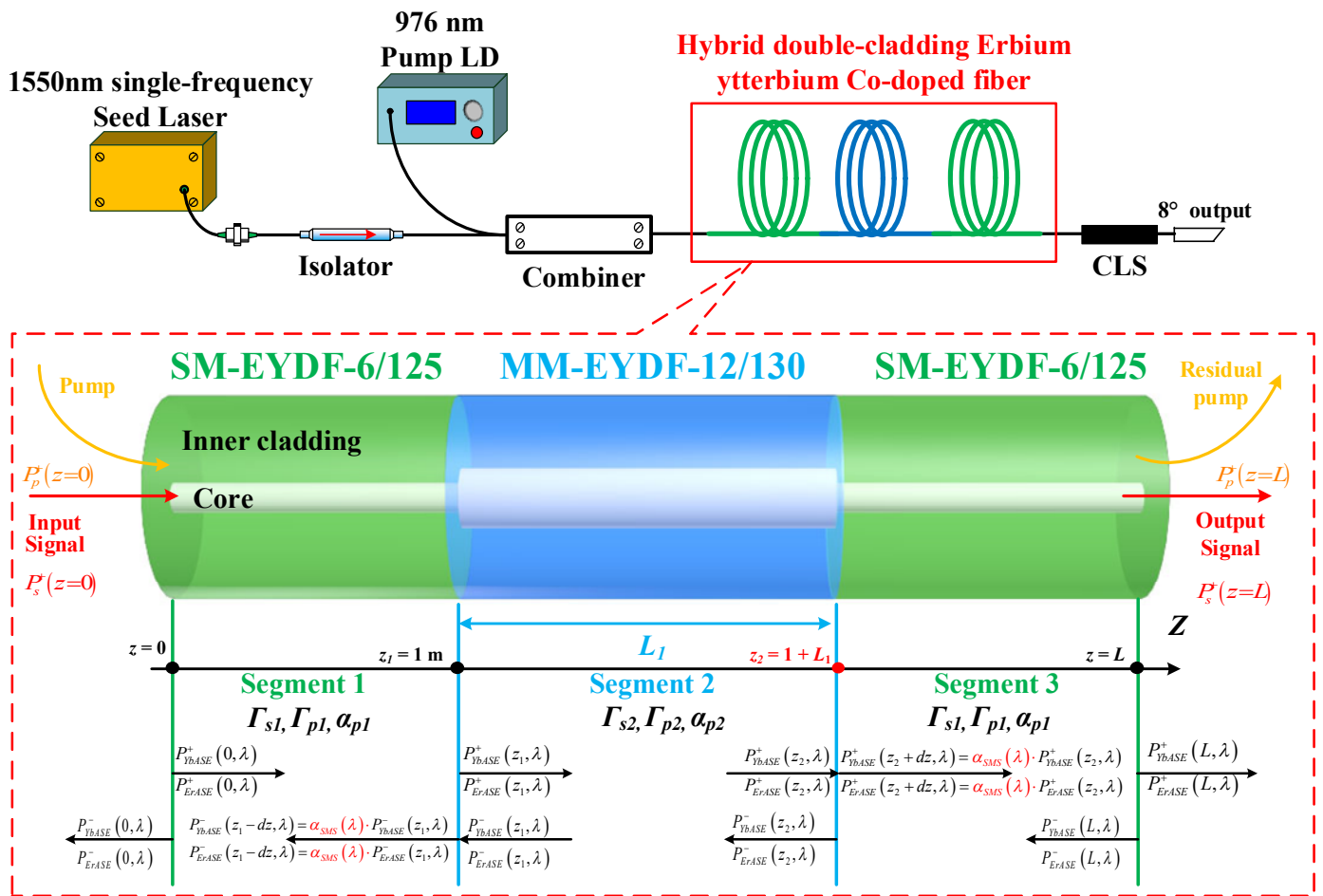


Figure 1. The schematic diagram of the hybrid EYDF amplifier. CLS, cladding light stripper.

3. Results and Analysis

3.1. Numerical Analysis of Hybrid EYDF Amplifier

The power scaling and ASE of the EYDF amplifier with hybrid or uniform fiber were numerically analyzed. The simulation model of the hybrid EYDF amplifier is shown in Figure 1. The total length L of the gain fiber is 3 m, for both the hybrid and uniform fiber. The multimode fiber is inserted into two segments of single-mode fiber. The distance between the multimode fiber and $z = 0$ is fixed at 1 m. The length of the multimode fiber is assumed to be L_1 . The seed and pump laser are forward coupled into the gain fiber at length position $z = 0$, and launched at $z = L$. The power of the seed and pump in the simulation are assumed to be 30 mW and 20 W, respectively. The output performance of hybrid gain fiber amplifier is affected by two aspects: one is the spectra modulation of the SMS structure, which can be obtained by analyzing the MMI effect; the other is the gain characteristics of the active fiber, which can be obtained by numerically analyzing the steady-state rate equations of the EYDF amplifier. The length of the multimode gain fiber is optimized by simulation. The core diameter and length of the multimode fiber have a significant influence on the transmission spectrum of the SMS structure due to the MMI effect. The modulation depth is related to the number of guiding modes N in the center multimode fibers. The number of guiding modes N can be estimated by the core diameter a , the working wavelength λ and the numerical aperture (NA), according to Equation (1) [21]. The V is normalized frequency. The core NA of MM-EYDF-6/125 is 0.2. If the working wavelengths are 1 and 1.5 μm , the number of guiding modes participating in multimode coherence are estimated to be 10 and 23, respectively. It can be inferred that the Yb-ASE at the 1- μm band has higher modulation depth than Er-ASE at the 1.5- μm band.

$$\begin{cases} N \approx \frac{V^2}{2} \\ V = 2\pi \frac{a}{\lambda} \cdot NA \end{cases} \quad (1)$$

The modulation property of SMS structure fiber was numerically analyzed by the BPM method [27]. Figure 2a is the transmission spectrum of the SMS structure with 5-cm multimode fiber. There is an obvious periodic modulation of the spectrum due to the MMI effect. The modulation of the MMI effect is not obvious in the 1.5-μm band because of insufficient guiding modes. The maximum modulation depth at the 1.5-μm band is only 3~4 dB, which is much lower than that of the 1-μm band where the Yb-ASE located. This phenomenon makes it possible to suppress Yb-ASE in the amplifier. The length of multimode fiber L_1 is related to the wavelength spacing $\Delta\lambda$ of the modulation spectrum. According to the literature [20], the wavelength interval $\Delta\lambda$ can be calculated by Equation (2):

$$\Delta\lambda = \frac{16n_{core}a^2}{(m-n)[2(m-n)-1]L_{MMF}} \quad (2)$$

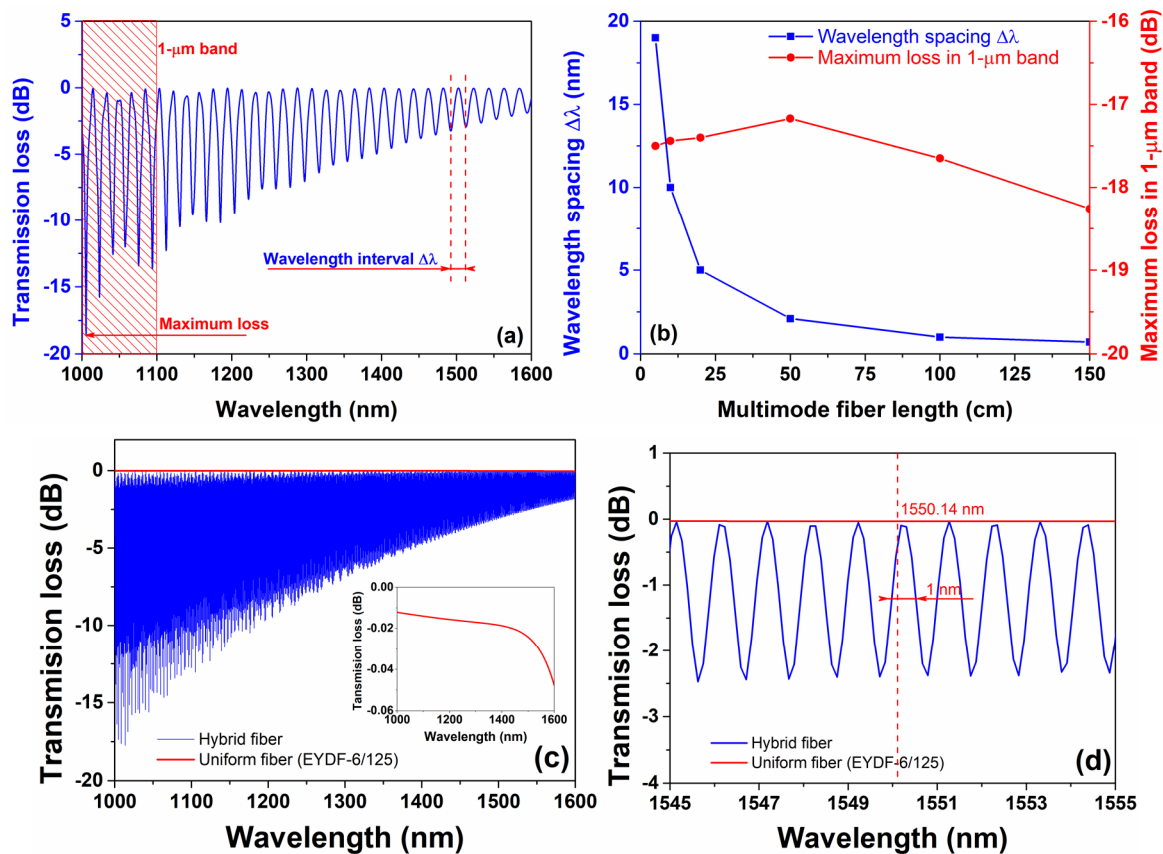


Figure 2. (a) The transmission spectrum of the active SMS with 5-cm multimode fiber; (b) the maximum loss in the 1-μm band and wavelength spacing with variation in multimode fiber length; (c) the transmission spectrum of the active SMS with 1-m multimode fiber. (Inset) the transmission loss of a uniform EYDF-6/125 fiber; (d) the zoomed transmission spectrum in the range of 1545~1555 nm.

Here, m and n are the order number of the linear polarization modes LP_{0m} and LP_{0n} , respectively. The wavelength interval decreases with the MM fiber length. A sufficiently small wavelength interval can avoid lasing at other wavelengths. The maximum loss in the 1-μm band and wavelength interval with variations in the multimode fiber length L_1 were simulated, which is shown in Figure 2b. When L_1 increases from 5 cm to 1.5 m, the wavelength interval decreases rapidly while the maximum loss increases slightly until the length is over 50 cm, then it decreases with the length increment. The multimode fiber length L_1 was selected to be 1 m to obtain sufficient loss and a suitable wavelength interval,

and the corresponding wavelength spacing was about 1 nm. The transmission spectrum of the active SMS with 1-m multimode fiber is plotted in Figure 2c. Because the wavelength of Yb-ASE is much shorter than that of Er-ASE, Yb-ASE can stimulate more transverse modes in the multimode fiber, and obtains more significant MMI effects. The maximum loss in the 1- μm band was 17.7 dB at 1013 nm, while it was only 2.3 dB at 1553 nm. The transmission loss of a uniform EYDF-6/125 was also simulated in the wavelength range of 1~1.6 μm , which is shown as a red line in the insertion in Figure 2c. The spectrum fluctuations of the uniform fiber were less than 0.04 dB. This comparison of the results demonstrates that the difference in transmission loss between the 1 and 1.5 μm bands is caused by the effect of multimode interference. The different transmission loss between the 1- μm and 1.5- μm band make it possible to suppress Yb-ASE in the amplifier. The transmission spectrum of the SMS is zoomed from 1545 to 1555 nm and plotted in Figure 2d to evaluate the loss of signal at 1550 nm. The transmission loss at 1550 nm is only 0.35 dB, and the full width at half maximum (FWHM) of the transmission peak is near 1 nm, which is equal to the wavelength interval. Although the transmission spectrum was periodically modulated, the loss value at spectral drops was still less than 2.5 dB and can be reduced by the gain property of the active fiber and the suppression of Yb-ASE. It can be inferred that this structure can not only be applied in narrow linewidth laser amplification, but also it could support laser amplification at the 1.55- μm band.

Based on the BPM analysis of the SMS structure, the output properties of the hybrid fiber amplifier were further simulated. Besides the mentioned pump absorption and core diameter, the steady state rate equations of EYDF and other parameters are referred to the literature [28,29]. The model of the simulation is plotted in Figure 1. The propagation equations for the signal power $P_s^+(z)$, pump power $P_p^+(z)$, Yb-ASE power $P^{\pm}_{YbASE}(z,\lambda)$ and Er-ASE power $P^{\pm}_{ErASE}(z,\lambda)$ are shown as follows [29]:

$$\begin{cases} \frac{dP_s^+(z)}{dz} = \{\Gamma_s[N_2(z)\sigma_{21}(\lambda_s) - N_1(z)\sigma_{12}(\lambda_s)] - \alpha(\lambda_s)\}P_s^+(z) + \frac{2hc^2}{\lambda^3}\Gamma_s N_2(z)\sigma_{21}(\lambda_s)m_s\Delta\lambda \\ \frac{dP_p^+(z)}{dz} = \{\Gamma_p[N_6(z)\sigma_{65}(\lambda_p) - N_5(z)\sigma_{56}(\lambda_p) - N_1(z)\sigma_{12}(\lambda_p)] - \alpha(\lambda_p)\}P_p^+(z) \\ \pm \frac{dP_{ErASE}^{\pm}(z,\lambda)}{dz} = \{\Gamma_s[N_2(z)\sigma_{21}(\lambda) - N_1(z)\sigma_{12}(\lambda)] - \alpha(\lambda)\}P_{ErASE}^{\pm}(z,\lambda) + \frac{2hc^2}{\lambda^3}\Gamma_s N_2(z)\sigma_{21}(\lambda)m_s\Delta\lambda \\ \pm \frac{dP_{YbASE}^{\pm}(z,\lambda)}{dz} = \{\Gamma_s[N_6(z)\sigma_{65}(\lambda) - N_5(z)\sigma_{56}(\lambda) - N_1(z)\sigma_{12}(\lambda)] - \alpha(\lambda)\}P_{YbASE}^{\pm}(z,\lambda) + \frac{2hc^2}{\lambda^3}\Gamma_s N_6(z)\sigma_{65}(\lambda)m_s\Delta\lambda \end{cases} \quad (3)$$

Here the symbol “ \pm ” represents forward (+) and backward (-) transmitted lights. The rate equations of the ytterbium and erbium energy system are referred to in the literature [29]. All the parameters in segment 1 are the same to those in segment 3. According to the fibers' specification, the signal overlap factor Γ_s of segment 1 and segment 2 were calculated to be 0.83 and 0.96, respectively, and the pump overlap factor Γ_p , which can be approximated as the area ratio of core to cladding, was 0.0023 and 0.0092, respectively. The pump absorption of these fibers was experimentally measured as mentioned above. The σ_{65} and σ_{56} are the emission and absorption cross-section of Yb-ions, respectively, and σ_{21} and σ_{12} are those of Er-ions. N_2 and N_1 are the population of the upper and lower energy levels of Er-ions, respectively. In the steady-state equations, the population of metastable levels $N_3 \approx 0$. The Er-ion concentration approaches $N_1 + N_2$. N_5 and N_6 are the population of the upper and lower energy levels of Yb-ions, respectively, and their summation is the Yb-ions concentration. According to the absorption coefficient and absorption cross-section, the Er-ions and Yb-ions concentration of SM-EYDF-6/125 in the simulation are 1.36×10^{24} and 1.29×10^{25} , respectively. The Er-ions and Yb-ions concentration of MM-EYDF-12/125 are 3.55×10^{24} and 3.83×10^{25} , respectively. The output power properties can be obtained in the simulation by substituting the fiber parameters at the corresponding position. It should be noted that since the signal light can pass through the SMS structure with almost no insertion loss (less than 0.1 dB), and because the inner cladding has the same diameter, the insertion loss in the SMS structure to the pump light is relatively small and was ignored. The additional loss caused by the MMI effect is marked as $\alpha_{SMS}(\lambda)$, which was obtained above by BPM analysis of the SMS structure. It is assumed that the MMI loss $\alpha_{SMS}(\lambda)$

affects the forward ASE power at the end of the multimode fiber position $z = z_2$, and reacts to the backward ASE power at $z = z_1$. So, the boundary condition of Yb-ASE and Er-ASE with MMI loss is shown in Equation (4). dz is the length unit that divides the fiber length.

$$\begin{cases} P_{ErASE}^+(z_2 + dz, \lambda) = \alpha_{SMS}(\lambda) \cdot P_{ErASE}^+(z_2, \lambda) \\ P_{YbASE}^+(z_2 + dz, \lambda) = \alpha_{SMS}(\lambda) \cdot P_{YbASE}^+(z_2, \lambda) \\ P_{ErASE}^-(z_1 - dz, \lambda) = \alpha_{SMS}(\lambda) \cdot P_{ErASE}^-(z_1, \lambda) \\ P_{YbASE}^-(z_1 - dz, \lambda) = \alpha_{SMS}(\lambda) \cdot P_{YbASE}^-(z_1, \lambda) \end{cases} \quad (4)$$

In Equation (4), the wavelength λ range of Er-ASE and Yb-ASE are 1000~1100 nm and 1500~1600 nm, respectively. The output property of the hybrid fiber amplifier can be obtained by adding the MMI loss $\alpha_{SMS}(\lambda)$ to the equations and solving them with the finite difference method [28]. The pump and signal power evolution in the hybrid and uniform fiber amplifier are plotted in Figure 3a. The launched signal power of the hybrid fiber amplifier with or without considering the MMI effect are both higher than the 4.52-W signal power obtained by the uniform fiber amplifier with the same fiber length and pump conditions due to its high pump absorption. Considering the spectral modulation effect of the SMS structure, the signal power in the hybrid amplifier (marked as hybrid fiber with MMI) was 5.51 W under 20 W pump power. However, the power calculated considering only the fiber size and doping concentration of the hybrid fiber, which is marked as the hybrid fiber without MMI in the figure, was 5.25 W, which is less than that with MMI by 0.26 W. The optical conversion efficiency of the hybrid fiber amplifier is 27.5%, which is 4.9% more efficient than that of the uniform one. The variation trend in the signal and pump light indicates that more gain and pump absorption can be provided by the multimode fiber. Comparing the signal in the hybrid fiber with and without MMI effect, the attenuation effect of the MMI effect on forward and backward ASE is inferred as another reason for obtaining higher efficiency in the hybrid fiber amplifier.

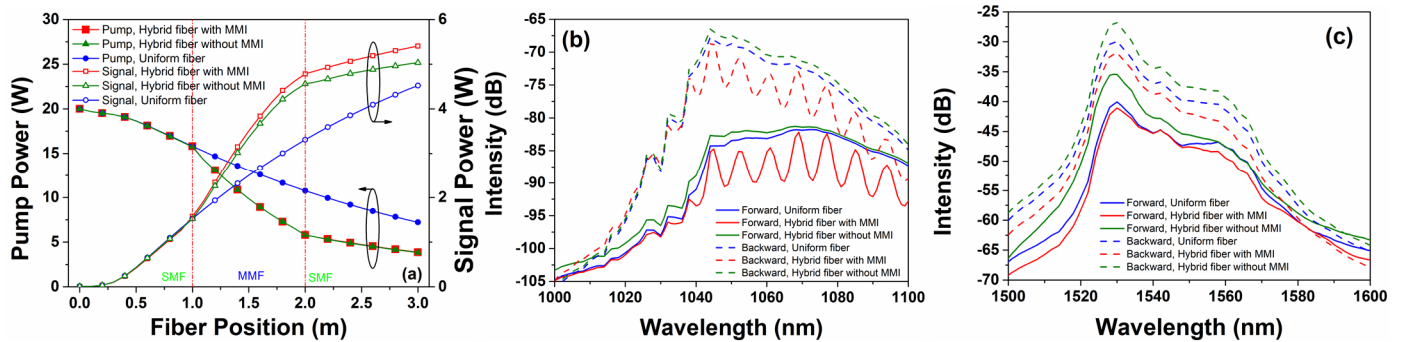


Figure 3. (a) Simulated pump and signal power evolution of amplifier with hybrid fiber and uniform fiber. (b) The simulation spectra at the 1- μ m band. (c) The simulation spectra at the 1.5- μ m band.

The reduction in backward and forward ASE by the MMI effect can improve the small-signal gain in segment 1 and the energy conversion between Er^{3+} and Yb^{3+} in segment 3, respectively. The signal power without MMI was 1.52 W at z_1 position, while the power with MMI was 1.57 W, which can be further demonstrated by the simulation spectra of the hybrid fiber amplifier at the 1- μ m and 1.5- μ m band. The forward spectra are represented by solid lines in the figure, and the backward spectra are dashed lines. Compared with the uniform fiber amplifier, the forward and backward Yb-ASE spectra of the hybrid fiber amplifier with MMI effect are periodically modulated in Figure 3b. However, the forward and backward Er-ASE at the 1.5 μ m band is hardly modulated, which is plotted in Figure 3c. These results demonstrate that the SMS structure has high transmission loss or are due to the modulation depth at the 1- μ m band. The forward and backward Yb-ASE without considering the MMI effect have the highest intensity because of the additional gain provided by the multimode fiber. This situation also appears in the Er-ASE spectra in Figure 3c. The additional gain increases the output power and ASE intensity at the same

time. However, the spectral modulation caused by the MMI effect suppresses the intensity of Yb-ASE. Although there are some spectral peaks in the 1040~1100 nm band, the forward Yb-ASE peak intensity was still suppressed by 0.5~2.9 dB by the MMI effect. The maximum suppression was 8.3 dB at 1073 nm. The backward Yb-ASE had the same trend and the maximum suppression was 8.1 dB at 1073 nm. The forward Er-ASE intensity decreased by only 1~1.6 dB. Although $\alpha_{SMS}(\lambda)$ in the 1.5- μm band has a loss of 2~3 dB, the Yb-ASE decrement improves the energy conversion between Er^{3+} and Yb^{3+} and avoids the Er-ASE decrement significantly. The backward Er-ASE intensity decreased by about 5 dB, which is the result of the interaction of additional gain and MMI modulation. In summary, the simulation results demonstrate that the hybrid EYDF with an SMS structure can suppress part of Yb-ASE.

3.2. Experimental Analysis of Hybrid EYDF Amplifier

Figure 1 presents a schematic diagram of the hybrid EYDF amplifier. The power performance and spectra properties were experimentally analyzed. The power scaling of hybrid and uniform EYDF amplifiers was recorded by an optical power meter (Thorlabs, S425C-L and PM100D) and is plotted in Figure 4a. The output power increases linearly with the pump power. The hybrid EYDF amplifier with 30 mW seed can launch 4.33 W of output power under a 20 W pump, and the corresponding slope efficiency is 22.3%. However, the slope efficiency of the typical uniform SM-EYDF-6/125 fiber amplifier with the same seed and fiber length is 19.6%, which is less than that of the hybrid EYDF amplifier by 2.7%. The experimental output power and slope efficiency were less than the theoretical results. We consider that this difference was caused by the fiber fusion loss in the signal laser, and the leakage of pump light due to no coating at the fusion point. In addition, the mismatch between the signal wavelength and the transmission spectrum peak of the SMS structure will also lead to the decrement in efficiency. Unfortunately, we cannot further improve the output power because of the limitations of the experimental conditions. Nevertheless, compared with the uniform fiber amplifier, the hybrid gain fiber amplifier has advantages in regard to both output power and slope efficiency. One of the reasons is that the insertion of multimode fiber adds extra gain. Another is that the MMI effect of the SMS structure can suppress Yb-ASE and promote pump energy transfer, which was demonstrated by the simulation results and following spectral measurement. The output spectra of the hybrid and uniform fiber amplifiers at the maximum output power were recorded by an optical spectrum analyzer (Anritsu, MS9701C) and are plotted in Figure 4b. The Yb-ASE intensity of the hybrid EYDF amplifier was decreased by more than 12 dB compared with that of the uniform fiber amplifier. The spectral results illustrate that the SMS structure has a good effect on Yb-ASE suppression and has the potential to alleviate the bottleneck effect in EYDF.

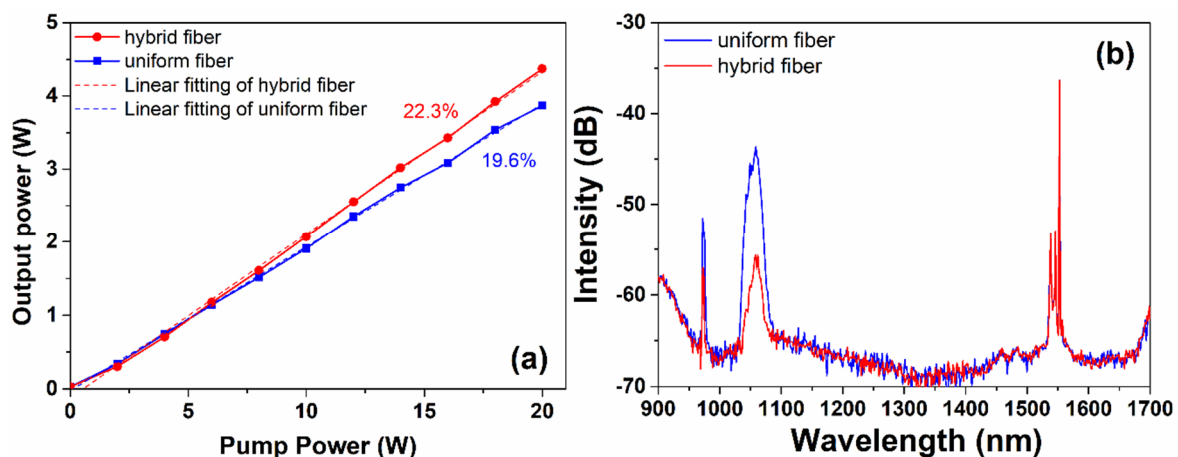


Figure 4. (a) The power scaling of the hybrid and uniform EYDF amplifier. (b) The output spectra of the hybrid and uniform fiber amplifier at the maximum output power in the 900 to 1700 nm region.

The zoomed spectra in the range of 1000 to 1100 nm are plotted in Figure 5a to analyze the detail of the Yb-ASE. The output spectrum of the hybrid fiber was obviously modulated. The maximum Yb-ASE suppression occurs at 1060.2 nm where the suppression intensity was 15.2 dB. However, the zoomed spectra in the 1530 to 1560 nm region, which is plotted in Figure 5b, demonstrate that this hybrid fiber amplifier cannot suppress the Er-ASE. The Er-ASE of the hybrid fiber amplifier was higher than that of the uniform fiber amplifier by 2~3 dB. These experimental results can be seen clearly in the insertion in Figure 5b, which is the zoomed spectra around 1535 nm with a 7 nm range. The Yb-ASE suppression promotes the pump power transfer and the pump leakage from the non-coated bare fiber can improve the gain in the 1.5- μm band. At the same time, the multimode fiber length variation caused by the instability in the fiber temperature may increase the signal light loss. A signal with insufficient power cannot effectively extract the upper-level population of Er^{3+} , which will also increase the Er-ASE intensity. High quality coating treatment at the fusion point and accurate fiber temperature control may be a possible way to avoid this phenomenon.

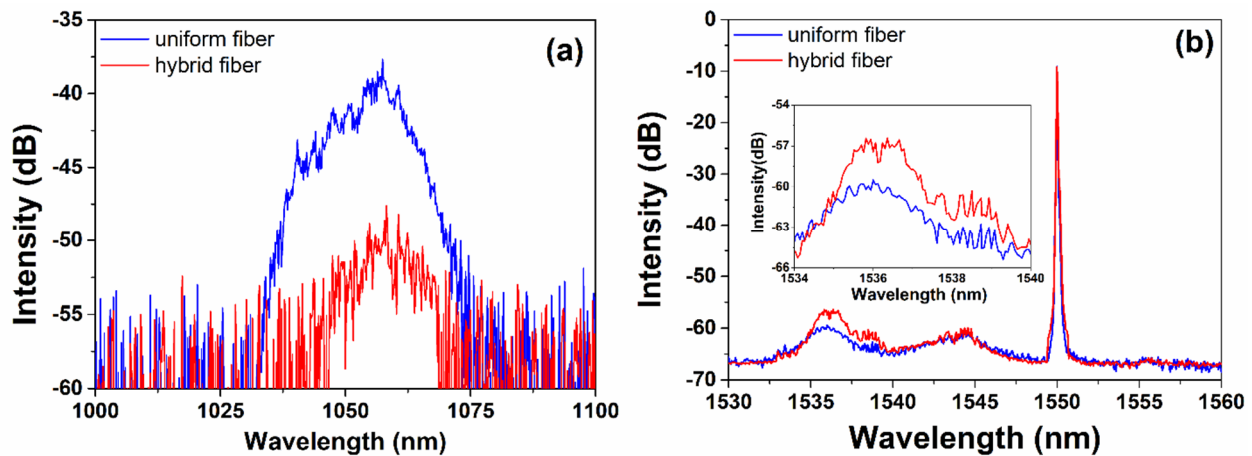


Figure 5. (a) Output spectra in the range of 1000 to 1100 nm. (b) The output spectra of the hybrid and uniform fiber amplifier in the 1530 to 1560 nm region. The insertion is the zoomed spectra in the range of 1534 to 1540 nm.

4. Conclusions

In this work, we studied a hybrid double cladding EYDF amplifier with an SMS active fiber. The SMS fiber structure consists of three segments of EYDF. The power performance and the spectra properties were theoretically and experimentally analyzed. The results for the hybrid fiber amplifier were compared with those of the uniform fiber amplifier. The simulation results demonstrate that the Yb-ASE of the hybrid fiber amplifier can be suppressed by over 10 dB due to high transmission loss in the SMS structure in the 1- μm band. The slope efficiency can also be improved because of the extra gain of multimode fiber. Based on the theoretical analysis, the hybrid EYDF amplifier and the typical uniform fiber amplifier were compared using experimental analysis. The Yb-ASE intensity of the hybrid fiber amplifier was suppressed by more than 12 dB, and the slope efficiency was increased by 2.7% compared with the typical uniform fiber amplifier. Although the Er-ASE increased about 2~3 dB, this hybrid EYDF amplifier has great advantages in regard to Yb-ASE suppression. This provides a possible technical path to suppress Yb-ASE and improve the amplification efficiency in the EYDF amplifier.

Author Contributions: Conceptualization, X.B.; Formal analysis, M.W. and Y.Y.; Methodology, X.B.; Resources, X.B.; Software, M.W.; Supervision, Z.L. and W.J.; Writing—review and editing, X.B. All authors have read and agreed to the published version of the manuscript.

Funding: This work was supported by the Natural Science Foundation of the Inner Mongolia Autonomous Region of China (2020BS06002, 2021BS06002), the Key Technology Research projects in the Inner Mongolia Autonomous Region (2021GG0274) and the scientific research projects of the Inner Mongolian higher educational system (NJZY21290).

Institutional Review Board Statement: Not applicable.

Informed Consent Statement: Not applicable.

Data Availability Statement: Data underlying the results presented in this paper are not publicly available at this time but may be obtained from the authors upon reasonable request.

Conflicts of Interest: The authors declare no conflict of interest.

References

1. Frehlich, R.; Hannon, S.M.; Henderson, S.W. Coherent Doppler lidar measurements of winds in the weak signal regime. *Appl. Opt.* **1997**, *36*, 3491–3499. [[CrossRef](#)] [[PubMed](#)]
2. Shi, W.; Fang, Q.; Zhu, X.; Norwood, R.A.; Peyghambarian, N. Fiber lasers and their applications. *Appl. Opt.* **2014**, *53*, 6554–6568. [[CrossRef](#)] [[PubMed](#)]
3. Jeong, Y.; Sahu, J.K.; Soh, D.B.; Codemard, C.A.; Nilsson, J. High-power tunable single-frequency single-mode erbium:ytterbium codoped large-core fiber master-oscillator power amplifier source. *Opt. Lett.* **2005**, *30*, 2997–2999. [[CrossRef](#)] [[PubMed](#)]
4. Bai, X.; Sheng, Q.; Zhang, H.; Fu, S.; Shi, W.; Yao, J. High-Power All-Fiber Single-Frequency Erbium–Ytterbium Co-Doped Fiber Master Oscillator Power Amplifier. *IEEE Photonics J.* **2015**, *7*, 1–6. [[CrossRef](#)]
5. Jeong, Y.; Harker, A.; Lovelady, M.; Piper, A.; Yoo, S.; Codemard, C.; Nilsson, J.; Sahu, J.K.; Payne, D.N.; Horley, R.; et al. Erbium:Ytterbium Codoped Large-Core Fiber Laser With 297-W Continuous-Wave Output Power. *IEEE J. Sel. Top. Quantum Electron.* **2007**, *13*, 573–579. [[CrossRef](#)]
6. Kuhn, V.; Kracht, D.; Neumann, J.; Weßels, P. Dependence of ErYb-codoped 1.5 μ m amplifier on wavelength-tuned auxiliary seed signal at 1 μ m wavelength. *Opt. Lett.* **2010**, *35*, 4105–4107. [[CrossRef](#)]
7. Sobon, G.; Kaczmarek, P.; Antonczak, A.; Sotor, J.; Abramski, K.M. Controlling the 1 μ m spontaneous emission in ErYb co-doped fiber amplifiers. *Opt. Express* **2011**, *19*, 19104–19113. [[CrossRef](#)] [[PubMed](#)]
8. Sobon, G.; Sliwinska, D.; Kaczmarek, P.; Abramski, K.M. Er/Yb co-doped fiber amplifier with wavelength-tuned Yb-band ring resonator. *Opt. Commun.* **2012**, *285*, 3816–3819. [[CrossRef](#)]
9. Han, Q.; He, Y.; Sheng, Z.; Zhang, W.; Ning, J.; Xiao, H. Numerical characterization of Yb-signal-aided cladding-pumped ErYb-codoped fiber amplifiers. *Opt. Lett.* **2011**, *36*, 1599–1601. [[CrossRef](#)] [[PubMed](#)]
10. Han, Q.; Yao, Y.; Chen, Y.; Liu, F.; Liu, T.; Xiao, H. Highly efficient Er/Yb-codoped fiber amplifier with an Yb-band fiber Bragg grating. *Opt. Lett.* **2015**, *40*, 2634–2636. [[CrossRef](#)] [[PubMed](#)]
11. Creeden, D.; Pretorius, H.; Limongelli, J.; Setzler, S.D. Single frequency 1560 nm Er:Yb fiber amplifier with 207W output power and 50.5% slope efficiency. In *Fiber Lasers XIII: Technology, Systems, and Applications*; SPIE LASE: San Francisco, CA, USA, 2016; Volume 9728, p. 97282. [[CrossRef](#)]
12. Booker, P.; Caspary, R.; Neumann, J.; Kracht, D.; Steinke, M. Pump wavelength dependence of ASE and SBS in single-frequency EYDFAs. *Opt. Lett.* **2018**, *43*, 4647–4650. [[CrossRef](#)] [[PubMed](#)]
13. Fu, S.; Shi, G.; Sheng, Q.; Shi, W.; Zhu, X.; Yao, J.; Norwood, A.; Peyghambarian, N. Dual-wavelength fiber laser operating above 2 μ m based on cascaded single-mode-multimode-single-mode fiber structures. *Opt. Express* **2016**, *24*, 11282–11289. [[CrossRef](#)] [[PubMed](#)]
14. Mohammed, W.; Mehta, A.; Johnson, E.G. Wavelength Tunable Fiber Lens Based on Multimode Interference. *J. Light. Technol.* **2004**, *22*, 469–477. [[CrossRef](#)]
15. Chen, Y.; Han, Q.; Liu, T.; Xiao, H. Wavelength Dependence of the Sensitivity of All-Fiber Refractometers Based on the Singlemode–Multimode–Singlemode Structure. *IEEE Photonics J.* **2014**, *6*, 1–7. [[CrossRef](#)]
16. Gong, Y.; Zhao, T.; Rao, Y.-J.; Wu, Y. All-Fiber Curvature Sensor Based on Multimode Interference. *IEEE Photonics Technol. Lett.* **2011**, *23*, 679–681. [[CrossRef](#)]
17. Zhao, Y.; Li, X.-G.; Meng, F.-C.; Zhao, Z. A vibration-sensing system based on SMS fiber structure. *Sens. Actuators A Phys.* **2014**, *214*, 163–167. [[CrossRef](#)]
18. Zhao, Y.; Cai, L.; Li, X.-G.; Meng, F.-C.; Zhao, Z. Investigation of the high sensitivity RI sensor based on SMS fiber structure. *Sens. Actuators A Phys.* **2014**, *205*, 186–190. [[CrossRef](#)]
19. Tang, J.; Pu, S.; Dong, S.; Luo, L. Magnetic Field Sensing Based on Magnetic-Fluid-Clad Multimode-Singlemode-Multimode Fiber Structures. *Sensors* **2014**, *14*, 19086–19094. [[CrossRef](#)]
20. Mohammed, W.S.; Smith, P.W.E.; Gu, X. All-fiber multimode interference bandpass filter. *Opt. Lett.* **2006**, *31*, 2547–2549. [[CrossRef](#)] [[PubMed](#)]
21. Zhu, X.; Schulzgen, A.; Li, H.; Li, L.; Han, L.; Moloney, J.V.; Peyghambarian, N. Detailed investigation of self-imaging in large-core multimode optical fibers for application in fiber lasers and amplifiers. *Opt. Express* **2008**, *16*, 16632–16645. [[CrossRef](#)] [[PubMed](#)]

22. Soldano, L.B.; Pennings, E.C.M. Optical multi-mode interference devices based on self-imaging: Principles and applications. *J. Light. Technol.* **1995**, *13*, 615–627. [[CrossRef](#)]
23. Bai, X.; Sheng, Q.; Fu, S.; Xie, Z.; Shi, W.; Yao, J. Compact bi-direction pumped hybrid double-cladding EYDF amplifier. In Proceedings of the CLEO: Science and Innovations, San Jose, CA, USA, 13–18 May 2018; p. SM2N.7. [[CrossRef](#)]
24. Bai, X.; Wang, M.; Yang, Y.; Liu, Z.; Jia, W. Experimental and theoretical analysis on pump spectral propriety of single frequency Erbium-Ytterbium co-doped fiber amplifier. *J. Phys. Commun.* **2021**, *5*, 105005. [[CrossRef](#)]
25. Silva, S.; Frazão, O.; Viegas, J.; Ferreira, L.; Araújo, F.M.; Malcata, F.; Santos, J.L. Temperature and strain-independent curvature sensor based on a singlemode/multimode fiber optic structure. *Meas. Sci. Technol.* **2011**, *22*, 085201. [[CrossRef](#)]
26. Lia, E.; Wang, X.; Zhang, C. Fiber-optic temperature sensor based on interference of selective higher-order modes. *Appl. Phys. Lett.* **2006**, *89*, 091119. [[CrossRef](#)]
27. Wu, Q.; Semenova, Y.; Wang, P.; Farrell, G. High sensitivity SMS fiber structure based refractometer – analysis and experiment. *Opt. Express* **2011**, *19*, 7937–7944. [[CrossRef](#)]
28. Han, Q.; Liu, T.; Lu, X.; Ren, K. Numerical methods for high-power Er/Yb-codoped fiber amplifiers. *Opt. Quantum Electron.* **2014**, *47*, 2199–2212. [[CrossRef](#)]
29. Dong, L.; Matniyaz, T.; Kalichevsky-Dong, M.T.; Nilsson, J.; Jeong, Y. Modeling Er/Yb fiber lasers at high powers. *Opt. Express* **2020**, *28*, 16244–16255. [[CrossRef](#)]